Electromagnetic Design and Simulation of a New Fusion Device

B. Dursun[1], E. Kurt[2]

[1]*Department of Electrics, Faculty of Technical Education, Gazi University,*
06500 Teknikokullar, Ankara, Turkey
[2]*Department of Electrical and Electronics Engineering, Technology Faculty, Gazi University,*
06500 Teknikokullar, Ankara, Turkey
ekurt@gazi.edu.tr

Abstract—A new inertial electrostatic confinement (IEC) fusion device is proposed. The device contains two ion guns which feed the plasma media by deuterium ions. The device is designed in three dimensions and the finite difference method is applied to satisfy the boundary values of the cylindrical chamber. It is the first time that both the ions and electrons are simulated in this geometry by particle in cell (PIC) technique. Ions and electrons can interact with six bar-sized cathodes of the chamber and each other as a result of many-body problem. The device has a central dc current-carrying rod, which generates a homogeneous magnetic field surrounding the six cathodes. Thus we expect a better confinement compared to the conventional devices. The simulation records the real-time position and momentum by using the electromagnetic equations together with the momentum equations. The dynamics of the particles is seen to be complicated with vibrations on the horizontal plane due to the field.

Index Terms—Electrostatic confinement, particle in cell, magnetic field, temperature.

I. INTRODUCTION

Inertial electrostatic confinement (IEC) devices are steady-state electrical machines, which are used for the neutron lithography, steady-state x-ray production and fusion energy researches [1]–[4]. Since they operate at the order of kV scale fed by a dc source from the cathode, one should stabilize the device electrically in order to create a good plasma media. According to the literature the electrical power source should enable the confinement of the deuterium ions under the kV-scaled electrical potential [2], [3], [5]. In some applications, the chambers of the devices have cylindrical or spherical forms in relevance with the potential distribution which is used for the confinement of ions [6]–[8].

The device is initially vacuumed and filled with Deuterium gas up to 5 mTorr–10 mTorr. In order to balance the Deuterium ion density in the chamber, ion guns are attached to the vacuum chamber. A negative potential at the order of -30 kV accelerates the ions into the center of the chamber, then a confinement occurs with strong and weak x-rays due to the accelerations of ions and electrons. In order to obtain any fusion event, collisions of ions having certain kinetic energies should be provided.

From the studies of Elmore et al. [9], the equilibrium and stability problem of these devices were studied around 1959. The multi-well electrical potentials were proposed by Hirsh [10] and the initial experiments were performed as a result of his researches. Later on, Swanson and his colleagues explained electron injection phenomena and its effect to the potential structure inside the chamber [11]. During the first decade of 2000, some 2D computer experiments were carried out. In addition the principles of the IEC fusion reactors by ion density calculations were achieved [8], [12]. The effects of electron and ion injections were reported by Ohnishi and his colleagues [13]. These researches provided some information between the fusion events and the potential well stability. It was understood that the electrical potential pattern surrounding the cathode and the chamber center played an important role for the efficiency of the fusion device [4]. According to the results of Noborio et al [4], the simulations could give trajectories of the particles inside the chamber.

In one of the researches, the time-dependent solutions of the momentum and electrical equations were handled by Kurt on a two dimensional box [2]. Then, Kurt and his colleague introduced a new spherical IEC device with its three dimensional potential pattern [3], [6]. The electrical and magnetic features of the possible device materials were also determined for the cathode and dielectrics used for the cathode holder [3]. Recently, these simulation results have been used in the first experimental device of Turkey under the name SNRTC-IEC [1].

In the present paper, we purpose a new cylindrical-shape IEC device and some preliminary results of particle trajectories. The proposed design has a central current-carrying rod enabling circular magnetic field on the horizontal plane perpendicular to the cathode rods. The simulations are done in a real-time base. Section II gives a background on the analytical model of the new device. Next section presents some numerical simulations of the electromagnetic and momentum equations. Finally, the concluding section summarizes the main outcomes of the work.

II. THEORY AND MODELLING

The sketch of new IEC device is drawn in Fig. 1. It has

two ion guns positioned on the cylindrical outer wall of the chamber and these guns add Deuterium ions to the chamber. Note that the insulators preserve the ion guns from the ground of the chamber. The cathodes are designed at the middle of the chamber as six steel rods and enable the ions to be accelerated towards the center. All of them construct a hexagonal region on the horizontal plane and found a specific potential region for the electrically attractive potential well. The potential surface is mostly produced by these rods, where negative bias on the cathodes accelerates the ions from the outer part of the chamber towards the center. As an innovative effect, the chamber has a special central rod carrying a current I_0 in order to produce an azimuthal homogeneous magnetic field surrounding the central region (Fig. 1).
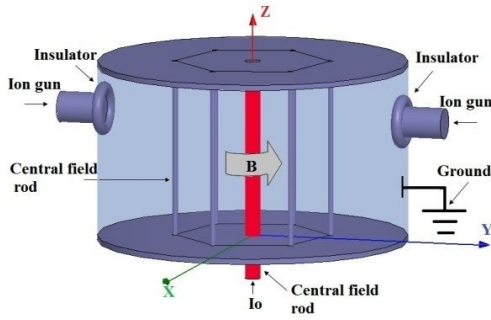
Fig. 1. The sketch of new IEC device.

Note that the central field rod is independent from the cathode voltage and its task is to adjust a circular magnetic field density B to the ions and electrons inside the chamber. Thus, the field will be maximum at the vicinity of center and decrease toward the peripheral region. Since the field creates a circular loop, charged particles (i.e. ions and electrons) are expected to have spiral trajectories along the field lines. Thus it will assist to have better particle density and plasma temperature. Here one should keep in mind that electrons and ions will make spirals in the opposite directions due to their opposite charges. The geometrical details of the chamber are summarized in Table I.

TABLE I. PHYSICAL FEATURES OF THE CHAMBER.

Cathode radius	0.3 m
Chamber radius	1 m
Chamber height	3 m

Different geometrical parameters can also be adjusted to the simulation however most of the results in this paper found for this geometry. By considering the above geometry, three dimensional real time simulations should be realized in terms of particle in cell method (PIC). According to literature, PIC method uses the ions and characterize a visual potential by taking account electrons to the potential well [14], [15]. However, in our case PIC includes electrons as real particles in addition to the ions, thus a many-body interaction is considered inside the chamber. Note that the interactions between the chamber components and particles are made by the finite difference method. The method includes several interactions such as cathode-ion, ion-ion, electron-ion and cathode-electron. Therefore the simulations require a long calculation time at computer. The model starts with the momentum equation in an electromagnetic media.
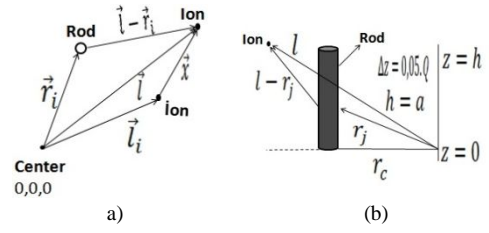
Fig. 2. Upper-view (a) and side-view of the interactions between cathode rod and ions in Cartesian coordinates (b).

Considering the position of the particles in vector form as in Fig. 2, one arrives at:

$$\frac{d^2\vec{l_i}}{dt^2} = E_i\left[\sum_{j=1}^{N}\frac{kQ_0\left(\vec{l_i}-\vec{r_j}\right)}{\left|\vec{l_i}-\vec{r_j}\right|^3} + \sum_{m=1}^{M-1}\frac{kq\left(\vec{l_i}-\vec{l_{im}}\right)}{\left|\vec{l_i}-\vec{l_{im}}\right|^3}\right] + $$
$$+B_i\left[\boldsymbol{k}\left(v_{ix}B_y - v_{iy}B_x\right)+\boldsymbol{j}v_{ix}B_x - \boldsymbol{i}v_{iz}B_y\right], \quad (1)$$

$$\frac{d^2\vec{l_e}}{dt^2} = E_e + \left[-\sum_{j=1}^{N}\frac{kQ_0\left(\vec{l_e}-\vec{r_j}\right)}{\left|\vec{l_e}-\vec{r_j}\right|^3} + \sum_{m=1}^{M-1}\frac{kq\left(\vec{l_e}-\vec{l_{em}}\right)}{\left|\vec{l_e}-\vec{l_{em}}\right|^3} - \right.$$
$$\left. -\sum_{m=1}^{M-1}\frac{kq\left(\vec{l_e}-\vec{l_{im}}\right)}{\left|\vec{l_e}-\vec{l_{im}}\right|^3}\right] + $$
$$+B_e\left[\boldsymbol{k}\left(v_{ex}B_y - v_{ey}B_x\right)+\boldsymbol{j}v_{ex}B_x - \boldsymbol{i}v_{ez}B_y\right], \quad (2)$$

where subscript i and e refers to ions and electrons, while m denotes the ion or electron index, j defines the index of rod element. In addition, unit vectors are shown by bold letters. The above equations also have electrical and magnetic scalar constants E and B. Since (1) and (2) include position and velocity components of particles, one can define all quantities after solving these equations, numerically. According to Fig. 2(b), the cathode rods are considered to be summed over $\cup z$ heights having a certain negative charge amount Q_0. The negative potential over the rods causes the total charge as follows, when the geometry is considered as a cylindrical capacitor

$$Q = \frac{2f\,H\vee_0 V_0}{6\ln(\frac{r_c}{r_a})}, with, Q = 6NQ_0\sqrt{a^2+b^2}, \quad (3)$$

Where V_0 denotes the negative potential, when H gives the chamber height. Note that (3) can be found after some mathematical manipulation following the boundary value problem of cylindrical chamber. The horizontal locations of rods are as follows:

$$\begin{cases} r_1(x,y)=r_a(1,0), \\ r_2(x,y)=0.5r_a(1,\sqrt{3}) \\ r_3(x,y)=-0.5r_a\left(1,\sqrt{3}\right), \\ r_4(x,y)=r_a(-1,0), \\ r_5(x,y)=-0.5r_a\left(1,\sqrt{3}\right), \\ r_6(x,y)=-0.5r_a\left(1,-\sqrt{3}\right). \end{cases} \quad (4)$$

For this analysis, we consider a particle near the central rod as in Fig. 3(a). According to Biot-Savard theorem, the current element on the central current rod produces the field density given by

$$\vec{B} = \int_0^L \frac{Idz\left[l_{0x}\boldsymbol{j} - l_{0y}\boldsymbol{i}\right]}{\left(\sqrt{l_{0x}^2 + l_{0y}^2 + \left(l_{0z} - l_{rz}\right)^2}\right)^3}. \quad (5)$$

(a)

(b)

(c)
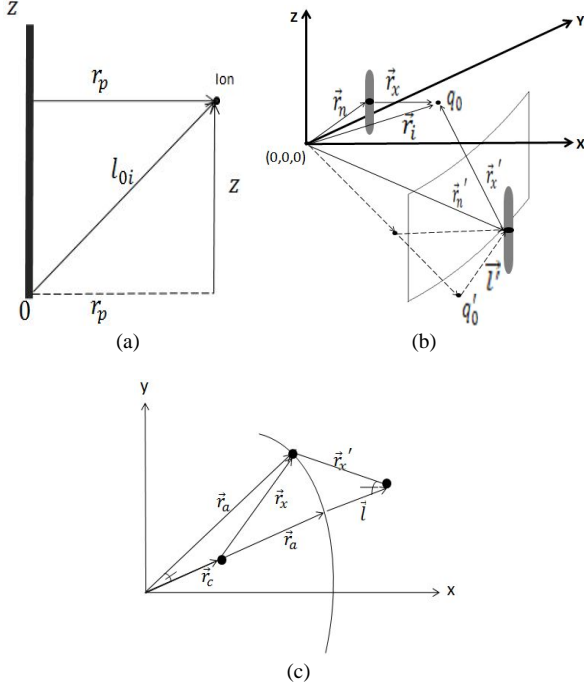
Fig. 3. An ith particle at the vicinity of central rod on vertical plane (a). The representation of the visual charge as boundary value problem (b). A specific condition to fulfill the boundary condition (c).

Formulation above leads to the field components with finite difference element $I\Delta z$ over total rod length. The z component of the central rod is indicated by l_{rz}. The dimensionless coefficients are defined as

$$\ddagger = \sqrt{\frac{l_0 m}{qk}}, r_a, \sqrt{\frac{q l_0}{km}}, \quad (6)$$

for time, length and magnetic field scales. Figure 3(b)–Fig. 3(c) show the visual charge method for the solution of boundary value problem, since the potential must vanish at the chamber boundaries. Thus all cathode rods and visual particles should be included into the potential expression. Therefore the position vector has an importance to determine the solution and also the special condition as seen in Fig. 3(c). From this figure, the total electrical potential of the system can be determined as

$$V_i = \sum \frac{-kQ}{|\vec{r}_x|} + \frac{Qk|\vec{r}_x'|}{|\vec{r}_x|} = \sum \frac{-kQ}{|\vec{r}_x|}\left\{|\vec{r}_x'| - 1\right\} =$$
$$= \sum -\frac{kQ}{\left(\sqrt{\left(r_{xi} - r_{ax} - l_x\right)^2 + \left(r_{yi} - r_{ay} - l_y\right)^2} - 1\right)\sqrt{\left(r_{xi} - r_{cx}\right)^2 + \left(r_{yi} - r_{cy}\right)^2}}, \quad (7)$$

where superscript (') defines the vector of visual particles and the sums are over the all cathode rods. According to the

detailed calculations, the visual charge caused by the visual cathode potential can be written as

$$Q' = \frac{Q|\vec{r}_x'|}{|\vec{r}_x|} = \frac{Q}{\left(\dfrac{1}{r_a} + \dfrac{l}{r_a^2}\right)|\vec{r}_x|}. \quad (8)$$

From (7)

$$\vec{E} = -\nabla V = -\boldsymbol{i}\,\frac{d}{dx}\frac{kQ}{|\vec{r}_x|}\left\{|\vec{r}_x'| - 1\right\} -$$
$$-\boldsymbol{j}\,\frac{d}{dy}\frac{kQ}{|\vec{r}_x|}\left\{|\vec{r}_x'| - 1\right\} - \boldsymbol{k}\,\frac{d}{dz}\frac{kQ}{|\vec{r}_x|}\left\{|\vec{r}_x'| - 1\right\}, \quad (9)$$

is obtained for electric field. The field components caused by cathodes can be written as

$$\begin{cases} E_x = \dfrac{-\left(x - r_{ax} - l_x\right)\sqrt{\left(x - r_{cx} +\right)^2 + \left(y - r_{cy} +\right)^2 + \left(z - z_a\right)^2}}{\left(x - r_{cx} +\right)^2 + \left(y - r_{cy} +\right)^2 + \left(z - z_a\right)^2} + \\[4mm] \dfrac{\left(x - r_{cx}\right)\left(\sqrt{\left(x - r_{ax} - l_x\right)^2 + \left(y - r_{ay} - l_y\right)^2 + \left(z - z_0\right)^2} - 1\right)}{\left(x - r_{cx} +\right)^2 + \left(y - r_{cy} +\right)^2 + \left(z - z_a\right)^2}, \\[4mm] E_y = \dfrac{-\left(y - r_{ay} - l_y\right)\sqrt{\left(x - r_{cx} +\right)^2 + \left(y - r_{cy} +\right)^2 + \left(z - z_a\right)^2}}{\left(x - r_{cx} +\right)^2 + \left(y - r_{cy} +\right)^2 + \left(z - z_a\right)^2} + \\[4mm] + \dfrac{\left(y - r_{cy}\right)\left(\sqrt{\left(x - r_{ax} - l_x\right)^2 + \left(y - r_{ay} - l_y\right)^2 + \left(z - z_0\right)^2} - 1\right)}{\left(x - r_{cx} +\right)^2 + \left(y - r_{cy} +\right)^2 + \left(z - z_a\right)^2}, \\[4mm] E_z = \dfrac{-\left(z - z_a\right)\sqrt{\left(x - r_{cx} +\right)^2 + \left(y - r_{cy} +\right)^2 + \left(z - z_a\right)^2}}{\left(x - r_{cx} +\right)^2 + \left(y - r_{cy} +\right)^2 + \left(z - z_a\right)^2} + \\[4mm] + \dfrac{\left(z - z_a\right)\left(\sqrt{\left(x - r_{ax} - l_x\right)^2 + \left(y - r_{ay} - l_y\right)^2 + \left(z - z_0\right)^2} - 1\right)}{\left(x - r_{cx} +\right)^2 + \left(y - r_{cy} +\right)^2 + \left(z - z_a\right)^2}. \end{cases} \quad (10)$$

Using the equations above, the electrical force can be determined after the boundary value calculations. From the numerical point of view, all simulations are realized in a MatLab code. An Intel Core i7 processor PC is used in the simulations. A typical simulation with 300 electrons and ions can be completed within 1 month in accordance with the simulation 400,000 simulation steps.

III. Results and Discussion

In order to show the potential well due to the negative potential of six cathodes, a contour-plot representation is given in Fig. 4. Here a different cathode distance from the center can be easily adjusted to the computer program in place of $r_c = 0.2$ m.

The rods have minimal potentials on the rods, however it decreases to zero by increasing distance from the center. There exists symmetry around the rods which can accelerate the particles homogeneously.

Some simulation results are given in Fig. 5. PIC method uses 600 particles in this study. Since the simulation time becomes drastically larger with increasing number of particles, one should limit the number of particles in the

computational cell in order to observe the position of ions and electrons. Figure 5 gives the position components of sample electrons near the center of chamber. The oscillations especially in *x*-direction dominate the motion due to the relatively low magnetic field on the horizontal plane, whereas the motion is regular in *z*-direction.

The position evaluation of a sample ion is presented in Fig. 6. Since ionic mass is much heavier than the electron's, its acceleration becomes lower than electron's. Thus it gets much time to evaluate its trajectory. Here the fluctuations remain on x-y plane again as in the case of electron due to the field. The cathodes with high potential attract the ions through the center for the fusion event. Some 3D appearances of electrons and ions in real-time trajectories are presented in Fig. 7.

According to these figures, an ion can travel everywhere in the chamber, however it reaches at the center after successive passes between the cathode rods. In addition, the interactions among the other ions can cause sudden changes in the directions of ions as seen in Fig. 7(a). Electrons are generally directed to one of the cathode rods due to their initial position and velocity. Note that these results are taken for a low magnetic field value. We expect that the increase in magnetic field can dominate the dynamics as successive strong oscillations of particles.

Fig. 4. The potential contour at $V = -100$ kV, $r_a = 1$ m, $r_c = 0.2$ m.
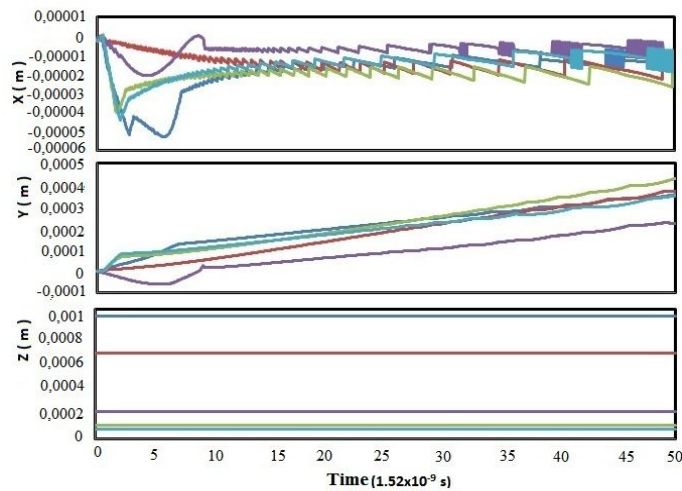
Fig. 5. The position components of 5 electrons in the chamber. $V = -15$ kV, $r_a = 1$ m, $r_c = 0.3$ m, $B_o = 0.073$ G.
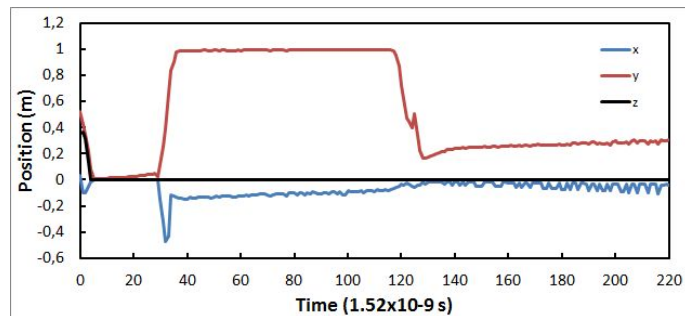
Fig. 6. The position components of a sample ion in the chamber. $V = -15$ kV, $r_a = 1$ m, $r_c = 0.3$ m, $B_o = 0.073$ G.

(a)

(b)
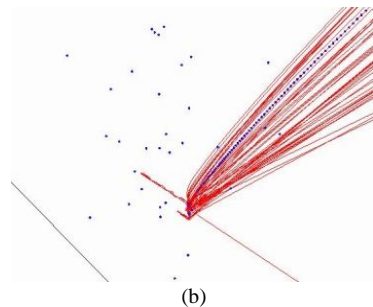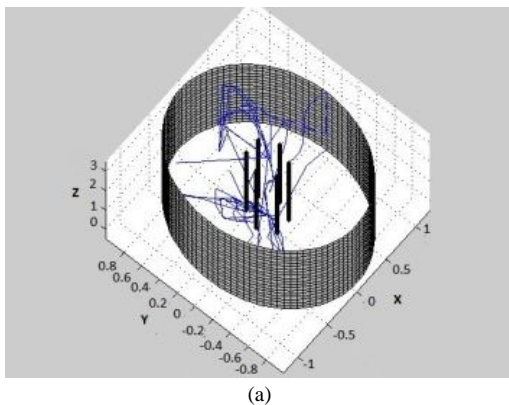
Fig. 7. Trajectory of an ion in the chamber ($V = -50$ kV, $B_o = 0.073$ G, $r_a = 1$ m and $r_c = 0.3$ m) (a). The ions (blue scattered points) and electrons (red) near the center inside the cathode rods $V = -15$ kV, $r_a = 1$ m, $r_c = 0.3$ m, $B_o = 0.073$ G (b).

Due to the increasing kinetic energy, ions can have higher possibility to adhere to the chamber walls. This simulation code can warn the user, when such a process occurs. In some different experimental devices, a number of corrosions can occur parallel to these results. In such a process, simply the ion exceeds the boundaries of the chamber and it is eliminated from the real time simulation.

IV. CONCLUSIONS

A new IEC reactor design and real-time simulations are performed. The device mainly includes a central current line which enables a homogeneous magnetic field in the central region of the chamber. It affects the attitudes of particles to exert vibrations in the central area. In this new simulation PIC uses electrons as individual particles to provide much realistic reactor apart from the earlier studies in which an averaged virtual potential was used. The trajectories are interesting due to their rapid position changes due to the interactions with the cathodes and other particles. In order to clarify the confinement process, a number of different simulations should be done in near future. From now it is obvious that the vibrations at the central region can lead to better confinement processes in the device. According to the results, increasing trend in kinetic energy causes negative impact on confinement, since ions may adhere to the walls or cathode rods. However we expect that homogeneous field can prevent such effects.

REFERENCES

[1] Y. Akgun, A. S. Bolukdemir, A. Alacakir, "Preliminary results of experimental studies from low pressure inertial electrostatic confinement device", *J. Fusion Energy*, vol. 32, no. 5, pp. 565–565, 2013.

[2] E. Kurt, "A stationary multi-component cathode modeling andion trajectories for an inertial electrostatic confinement fusion device", *Int. J. Energy Res.*, vol. 35, pp. 89–95, 2011. [Online]. Available: http://dx.doi.org/10.1002/er.1763

[3] E. Kurt, S. Arslan, M. E. Guven, "Effects of grid structures and dielectric materials ofthe holder in an Inertial Electrostatic Confinement (IEC) fusion device", *J. Fusion Energy*, vol. 30, no. 5, pp. 404–412, 2011. [Online]. Available: http://dx.doi.org/10.1007/s10894-011-9393-4

[4] K. Noborio, T. Sakai, Y. Yamamoto, "Investigation of spatial distribution of neutron production rate and its dependency on pressure in spherical IECF by one-dimensional simulations", in *20. Sym. Fusion Engin.*, 2003, pp. 328–331.

[5] E. Kurt, H. Kurt, U. Bayhan, "Ionization effects and linear stability in a coaxialplasma device", *Cent. Eur. J. Phys.*, vol. 7, no. 1, pp. 123–129, 2009. [Online]. Available: http://dx.doi.org/10.2478/s11534-008-0135-9

[6] E. Kurt, S. Arslan, "An inertial electrostatic confinement (IEC) device modeling and the effects of different cathode structures to the fields", *Energy Conv. Management*, (2012). [Online]. Available: http://dx.doi.org/10.1016/j.enconman.2011.12.033

[7] Yibin Gu, G. H. Miley, "Experimental study of potential structure in a spherical IEC fusion device", *IEEE Trans. Plasma Sci.*, vol. 28, no. 1, 2000. [Online]. Available: http://dx.doi.org/10.1109/27.842929

[8] S. K. Wong, N. A. Krall, "Potential well formation by injection of electrons with various energy distributions into a sphere or a slab", *Phys. Fluids B*, vol. 4, pp. 4140–4152, 1992. [Online]. Available: http://dx.doi.org/10.1063/1.860321

[9] W. C. Elmore, J.L. Tuck, K. M. Watson, "On the inertial-electrostatic confinement of a plasma", *Phys. Fluids*, vol. 2, pp. 239–246, 1959. [Online]. Available: http://dx.doi.org/10.1063/1.1705917

[10] R. L. Hirsch, "Inertial-electrostatic confinement of ionized fusion gases", *J. Appl. Phys.*, vol. 38, pp. 4522–4534, 1967. [Online]. Available: http://dx.doi.org/10.1063/1.1709162

[11] D. A. Swanson, B. E. Cherrington, J. T. Verdeyen, "Potential well formation in an inertial electrostatic plasma confinement device", *Phys. Fluids*, vol. 16, pp. 1939–1945, 1973. [Online]. Available: http://dx.doi.org/10.1063/1.1694238

[12] W. M. Nevins, "Can inertial electrostatic confinement work beyond the ion-ion collisional time scale?", *Phys. Plasmas*, vol. 2, pp. 3804–3819, 1995. [Online]. Available: http://dx.doi.org/10.1063/1.871080

[13] M. Ohnishi, K. H. Sato, Y. Yamamoto, K. Yoshikawa, "Correlation between potential well structure and neutron production in inertial electrostatic confinement fusion", *Nucl. Fusion*, vol. 37, no. 5, pp. 611–619, 1997. [Online]. Available: http://dx.doi.org/10.1088/0029-5515/37/5/I04

[14] Y. K Kurilenkov, V. P. Tarakanov, M. Skowronek, S. Y. Guskov, J Dufty, "Inertial electrostatic confinement and DD fusion at interelectrode media of nanosecond vacuum discharge. PIC simulations and experiment", *J. Phys. A: Math. Theor.*, vol. 42, 2009.

[15] M. Ohnishi, H. Osawa, K. Yoshikawa, K. Masuda, Y. Yamamoto, "Particle-in-Cell simulation of inertial electrostatic confinement fusion plasma", *Fusion Sci. Tech.*, vol. 39, no. 3, pp. 1211–1216, 2001.